Nanoscale

Accepted Manuscript

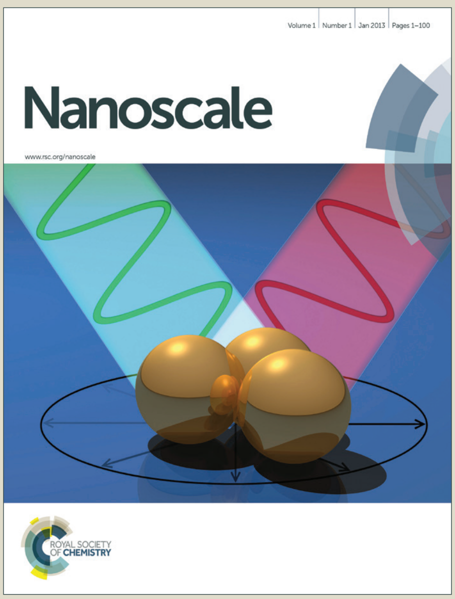

Cite this: DOI: 10.1039/c0xx00000x

www.rsc.org/xxxxxx

ARTICLE TYPE

Nanoscale

EELS Tomography in multiferroic nanocomposites: from spectrum images to the spectrum volume

Lluís Yedra,*[a,b] Alberto Eljarrat,[a] José Manuel Rebled,[a,c] Lluís López-Conesa,[a] Nico Dix,[c] Florencio Sánchez,[c] Sònia Estradé,[a,b] and Francesca Peiró[a]

Received (in XXX, XXX) Xth XXXXXXXXX 20XX, Accepted Xth XXXXXXXXX 20XX
DOI: 10.1039/b000000x

Electron Energy Loss Spectroscopy (EELS) in the Transmission Electron Microscope offers the possibility of extracting high accuracy maps of composition and electronic properties through EELS spectrum images (EELS-SI). Acquiring EELS-SI for different tilt angles, a 3D tomographic reconstruction of EELS information can be achieved. In the present work we show that an EELS spectrum volume (EELS-SV), a 4D dataset where every voxel contains a full EELS spectrum, can be reconstructed from the EELS-SI tilt series by the application of multivariate analysis. We apply this novel approach to characterize a nanocomposite material consisting on $CoFe_2O_4$ nanocolumns embedded in a $BiFeO_3$ matrix grown on $LaNiO_3$ buffered $LaAlO_3$ (001) substrate.

Introduction

Magnetoelectric (ME) multiferroics, as bulk single phase materials, first raised interest in the early sixties[1, 2], but their scarcity and weak or far too low temperature response caused research to languish. However, significant progress in multiferroic oxide thin films and the appearance of epitaxial composite thin films, where two phases with different ferroic properties are grown at once, have triggered a renewed and now huge interest in these functional materials. In particular, the composite thin films are robust multiferroic systems at room temperature yielding high magnetoelectric coefficients due to elastic coupling between the ferroelectric (FE) and ferri/ferromagnetic (FM) phases[3-5].

In the present work we consider FM $CoFe_2O_4$ (CFO) nanocolumns embedded in a FE $BiFeO_3$ (BFO) matrix grown on $LaNiO_3$ buffered $LaAlO_3$ substrate (BFO-CFO//LNO/LAO)[6]. This system, thoroughly studied[7], is a prototypical multiferroic vertical nanostructure. Studies in the past have shown the possibility of tailoring the properties of these materials by changing the substrate material, substrate orientation, ferroic phases and phase ratio, and film thickness[7-19].
The final functional properties of the nanocomposite being sensitive to the local composition, EELS can be much enlightening. Nevertheless, EELS is carried out in a 2D projection, while in the present case we require a 3D chemical characterization.

In transmission electron microscopy (TEM), 3D tomographic reconstruction can be achieved by acquiring a series of images at different tilt angles. A different approach is obtaining 3D chemical reconstructions from energy filtered images in the TEM (EFTEM)[20-22], and more recently, by acquiring EELS spectrum images (EELS-SI), each pixel containing a complete EELS spectrum[23, 24]. However, in both techniques only a limited amount of information is effectively reconstructed. In this paper we aim to derive a full EELS dataset in 4D, where every voxel of a whole volume contains a complete spectrum of energy losses, as schematized in Figure 1. By analogy to the spectrum image notation[25], we will name this 4D dataset as EELS spectrum volume (EELS-SV).

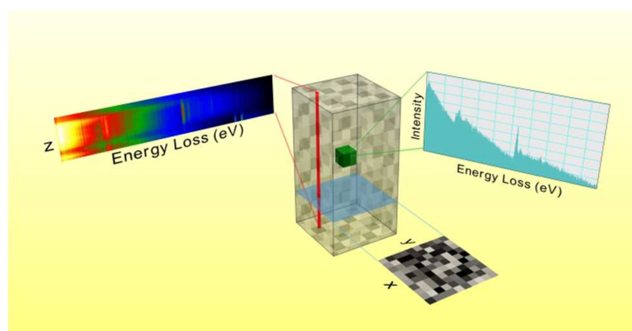

Figure 1: Schematic of the 4D dataset, the EELS spectrum volume, consisting of 3 spatial dimensions plus an additional energy loss dimension. Here it is presented along with an extracted xy spectrum image, a spectrum line along z direction and a single spectrum from an inner voxel.

G. Möbus et al.[20] suggested that the EELS-SV could be recovered by acquiring several tomography sets of EFTEM images, each set

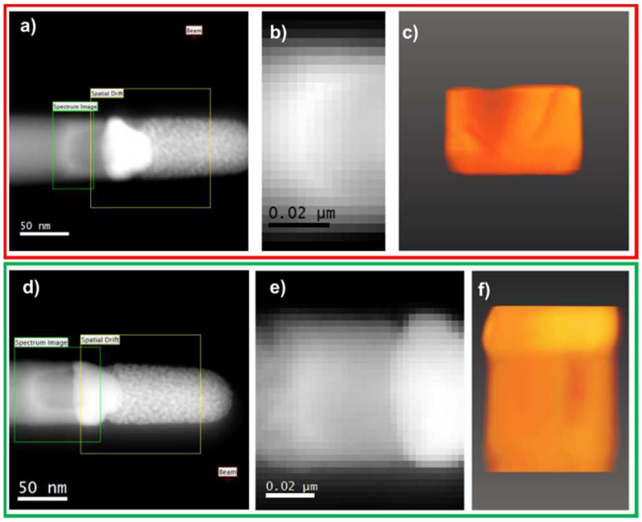

Figure 2: Areas of the nanoneedle used in the experiments. a) First experiment: HAADF survey image used for drift correction, b) coacquired HAADF signal used for alignment of the images and c) volume reconstruction. d) Second experiment: HAADF survey image used for drift correction, e) coacquired HAADF signal used for alignment of the images and f) volume reconstruction.

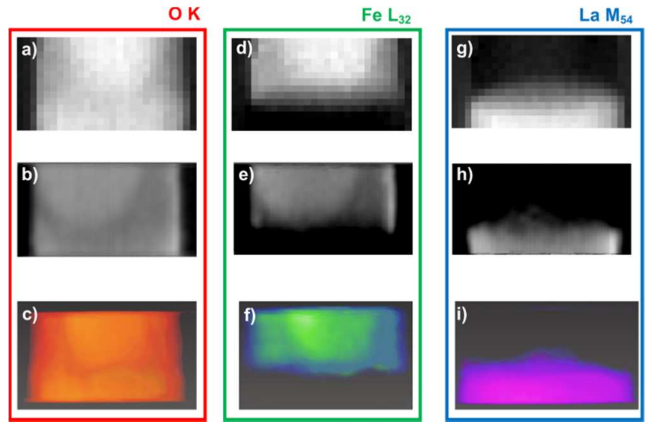

Figure 3: a) Original images and reconstructions in the preliminary experiment. Integrated O K signal for the image at -38.2º, b) orthoslice through the reconstructed volume and c) visualization of the reconstructed oxygen volume. d) Integrated Fe $L_{2,3}$ signal for the same image, e) orthoslice through the reconstructed Fe volume and f) visualization of the reconstructed volume. g) Integrated La $M_{4,5}$ signal, h) orthoslice through the reconstructed La volume and i) visualization of the reconstructed volume. Oxygen is found all over the sampled area, lanthanum is found in the bottom layer and iron on the top layer, where the BFO/CFO nanocomposite is.

consisting of a tilted series of images filtered for a specific energy, in a single tomography experiment. Then, a tomographic reconstruction would be required for each energy-filtered tilted series. This has already been applied for a few energy slices[26] but to recover a large region of the spectrum would require an enormous amount of EFTEM images for every tilt angle.

Our approach to EELS-SV reconstruction is used upon SI, thus taking a single SI for every tilt angle. It takes advantage of Multivariate Analysis (MVA), and more precisely of blind source separation (BSS)[27], to find a new spectral basis which can describe all the spectra in the dataset as a weighted sum of its components. Therefore only the 3D reconstructions of the weighting components will be necessary to recover the spectra in each voxel. We will apply this approach to analyze a BFO/CFO nanocomposites, enabling the characterization of a CFO nanocolumn embedded in BFO matrix.

Methods

The $BiFeO_3$ – $CoFe_2O_4$ epitaxial nanocomposite was deposited on a $LaNiO_3$-buffered $LaAlO_3$ (001) substrate by pulsed laser deposition. Detailed information about preparation conditions and properties is reported elsewhere[6].

EELS and HAADF were obtained in a JEOL JEM2010F coupled to a Gatan GIF spectrometer, operated at 200 kV, with a high resolution ultra narrow pole piece. The sample was prepared in a nanoneedle shape by Focused Ion Beam (FIB) in a FEI Strata 235 Dual Beam System. The nanoneedle was attached to the usual Omniprobe grid, only shortened at both ends to keep the maximum dimension below 1.5 mm in order to fit to a special sample holder (Fishione 2030 ultra-narrow gap tomography holder).

Multivariate Analysis was performed using Hyperspy[28, 29], a Python based EELS analysis toolbox. BSS was performed using the Bayesian Linear Unmixing software by N. Dobigeon[27]. The chosen software for image and tilt axis alignment and reconstruction were IMOD and Inspect3D. SIRT algorithm[30] was used for the reconstruction. Avizo imaging software was used for the final segmentation and visualization of the data.

Results and discussion

A nanoneedle sample was prepared by FIB from the BFO-CFO//LNO/LAO sample (see Supplementary Information, Figure S1). In order to test the suitability of the sample for EELS-SV reconstruction, a preliminary EELS-SI tomography experiment was carried out in a small area of the sample. The experiment consisted on the acquisition of 44 SI at tilt angles ranging from -66º to 62º. Figure 2 shows a HAADF survey image used for drift correction (2a), a coacquired HAADF signal used for alignment of the images (2b) and the reconstructed volume from the HAADF signal (2c). The dataset was denoised using Principal Components Analysis (PCA)[31] and the extracted edge intensities for O K, Fe $L_{2,3}$ and La $M_{4,5}$ were measured for each EELS-SI (Figure S3 in the supporting information). Other elements present in the dataset (Co and Ni) were not exploitable due to their low signal. As an example, Figure 3 displays in the following order original edge intensity maps from the projection at -38.2º, orthoslices through the reconstructed volume and a direct visualization of the reconstructed volume for oxygen, iron and lanthanum. If the necessary assumption that the intensities in the extracted maps are monotonically proportional to the amount of each element and the thickness of the sample (as discussed in the supporting information) is fulfilled, the orthoslices through the reconstruction should be proportional to the density of each element. Taking this into account, the intensities observed in Figure 3 can be interpreted as follows: the two higher intensities in the oxygen maps correspond to CFO and LAO/LNO, with densities of 54 atoms/nm^3 and 55 atoms/nm^3 respectively. BFO has an oxygen density of 48 atoms/nm^3 and therefore appears darker. The same reasoning applies to iron, with a concentration of 27 atoms/nm^3 in CFO and 16 atoms/nm^3 in BFO. Thanks to

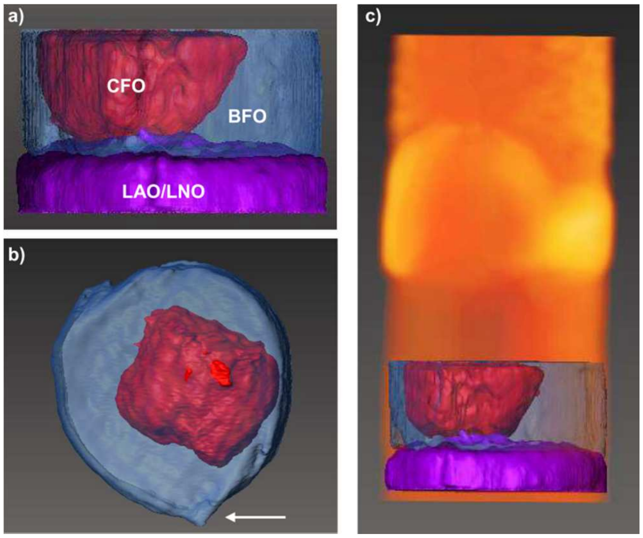

Figure 4: Visualization of the reconstruction in the preliminary EELS-SI tomography experiment. a) Direct visualization of the reconstructed and segmented volume. In purple the LAO/LNO substrate, in blue the iron and in red the CFO nanocolumn b) Axial view where the square section of the nanocolumn is observed (the bottom right side marked with the arrow is distorted due to the proximity to the limits of the reconstructed volume). c) Position of the reconstructed area using EELS signal with respect to the tip of the nanoneedle reconstructed from the HAADF survey image. In red the CFO nanocolumn extracted from O data.

these differences in concentration and following the procedure explained in reference[24], the three expected regions (LAO/LNO, BFO and CFO) could be separated in EELS maps and the subsequent segmentation of the areas of interest render the volumes presented in Figure 4. (See the supporting information for the movie and a full explanation and discussion of the procedure).

First, the sample stability was confirmed (despite the long duration of the experiment to acquire the whole tilt series of EELS-SI) and the EELS signal is proved adequate for tomographic reconstruction of the sample. In a second step, the tomographic acquisition was carried out in a wider region of the nanoneedle as shown in Figure 2d, 2e and 2f. For this second EELS-SI dataset comprising the whole multiferroic structure, the aim of data treatment was the reduction of the dataset to independent components. First the noise was reduced using PCA and then Blind Source Separation (BSS) was used to retrieve the independent components as explained in the supporting information. It is important that the components have physical meaning, so they can fulfill the projection requirement and be reconstructed using the usual tomography techniques.

The main three independent components of the dataset, assigned to background contribution, iron oxide and lanthanum oxide respectively are shown in Figure 5a. If we assume that each spectrum image is a weighted sum of these three independent components, each EELS-SI can be decomposed in three images corresponding to the weighting factors for the three independent components. Therefore, the whole EELS SI dataset was transformed to three new datasets suitable for tomographic reconstruction algorithms (for a thorough description see supporting information). The results of these reconstructions are shown in Figure 5b for the three components as labeled in Figure 5a and their superposition, which clearly corresponds to the

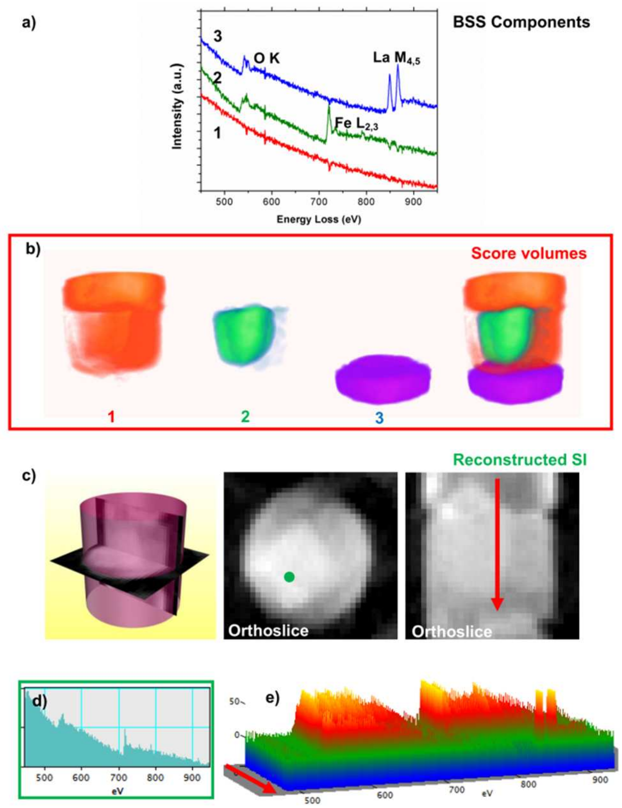

Figure 5: EELS-SV reconstruction procedure. a) Components of the spectrum according to BSS numbered as 1 – Thickness, 2 – Fe oxide and 3 – La oxide. b) 3D reconstructions of the 3 components extracted from Blind Source Separation (BSS), corresponding to the 3D score matrixes of the components, plus an overlapped image of the three. c) Schematic representation of two orthoslices and reconstructed SI for a transversal orthoslice (z=16) and a longitudinal orthoslice (y=16). d) Single spectrum extracted from the transversal orthoslice (green spot) and e) spectrum line along the red arrow in the longitudinal orthoslice reconstructed SI with its background subtracted by a power law before the O K edge.

whole volume in Figure 2f. A fourth component representing the noise in the vacuum was also retained for calculations, but its contribution will not be presented in the reconstructions.

At this point, the EELS-SV is already available, as the spectrum in each voxel can be calculated with the components and the three weighting factors corresponding to each component. In particular, we can retrieve an EELS-SI in any section of the EELS-SV by calculating the corresponding through the EELS-SV. From a SV of 32x32x36 spectra, the transversal orthoslice in Figure 5c shows the plane z=16, with a single spectrum extracted at the (15,12,16) voxel in Figure 5d. A spectrum line along the red arrow in the transversal orthoslice y=16 is shown in Figure 5e with its background subtracted by a power law.

To prove the validity of the voxel specific spectra, we integrate along the thickness, i.e., we calculate a new projection, to see whether the results are equivalent to the experimental data obtained in the microscope. In Figure 6, elemental maps of edge intensities for O, Fe and La extracted according to Figure 3 from three different sources are presented: from the original SI corresponding to 0º of tilt (6a), from the SI recalculated with the corresponding BSS components (6b) and from projection SI calculated from the reconstructed 4D EELS-SV (6c). The distribution of the elements (O, Fe and La) and the shape of the

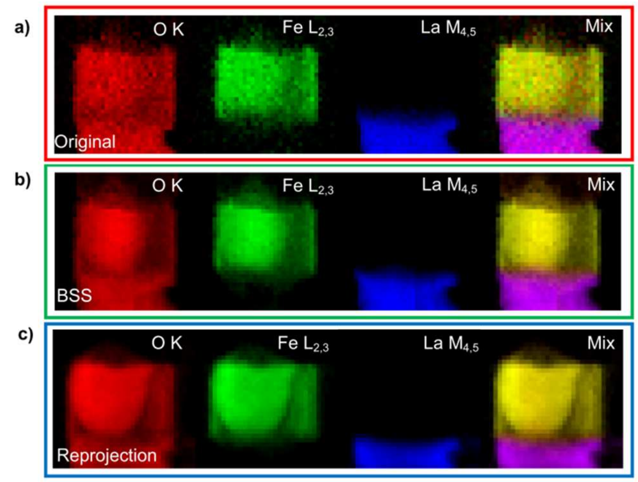

Figure 6: Comparison of the extracted edge intensities between a) the original projection at 0° tilt angle, b) the spectrum image at 0° built from the BSS components and c) the spectrum image built from projections of the EELS-spectrum volume (in all the images it can be observed that the gold deposited on the tip of the needle during FIB preparation masked the EELS signal at the top of the CFO nanocolumn).

CFO nanocolumn remain unaltered when reconstructed after the MVA analysis, as well as, the new EELS-SI from the projection of the reconstructed dataset compared to the original one. The small differences, observed in the border of the CFO nanocolumn, can be attributed to the alignment and reconstruction process (the procedure is sensitive to tomographic reconstruction artifacts), which results in a slight delocalization of the signals.

Regarding thickness related problems, the importance of nanoneedle-shaped preparation[32,33] through FIB is to be stressed, as the thickness of the sample was kept roughly constant throughout the experiment, therefore avoiding the signal drop at high angle expected in a conventional lamella preparation due to an increase in effective thickness as a consequence of the tilt angle. The intensity drop would have affected the monotonicity of the signals related to thickness, invalidating the reconstruction process. On the other hand, it must be noted that the spectrum calculated for each voxel contains information about the whole thickness of the sample, as it is reflected in the BSS components. However, we have proven that the elemental information is not compromised.

It is important to highlight that, to preserve the quality of the data, special care must be taken in the MVA analyses applied[34] both the PCA for noise reduction and the further BSS.

The data acquisition process is the same for the reported EELS-SI tomography[23, 24] and the method we propose. However, the recovery of the SV enables 3D visualization of properties that would be otherwise impossible to reconstruct, as they fail the projection requirement; namely, the fine structure of edges. While in the already established EELS-SI tomography every property in the spectrum needed to be extracted prior to reconstruction, in the new dataset it is possible to extract any information in the volume without having to further reconstruct it in 3D. Moreover, the new 4D dataset enables the use of local background averaging[34] in 3D for signal extraction.

Conclusions

In summary, EELS SI tomography has been shown capable of reconstructing the three dimensional structure of a nanocomposite sample as in conventional STEM-HAADF tomography, but adding a fourth dimension corresponding to chemical composition in a quantitative approach. In this case, CFO columns were properly reconstructed in a BFO matrix grown on a LNO/LAO substrate. Moreover, the feasibility of reconstructing EELS spectrum volumes (EELS-SV) such as those in Figure 1 has been shown and applied to extract single spectra from the inside of the nanocomposite sample, a step beyond the EELS-SI tomography and more accurate if compared to conventional SI, which integrates information all along the thickness of the sample. This approach could be extended to other spectroscopies.

The present work proves the great potential of EELS tomography for the characterization of nanostructured materials, especially if we take into account that the results shown here were not acquired using an ultrafast reading spectrometer, neither an aberration-corrected TEM.

Notes and references

[a] *Laboratory of Electron Nanoscopies (LENS)- MIND/IN2UB, Dept. d'Electrònica, Universitat de Barcelona, C/Martí i Franquès 1, 08028 Barcelona, Spain; E-mail: llyedra @el.ub.edu*
[b] *CCiT, Scientific and Technological Centres, Universitat de Barcelona, C/Lluís Solé i Sabaris 1, 08028 Barcelona, Spain.*
[c] *Institut de Ciència de Materials de Barcelona (ICMAB-CSIC), Campus de la UAB, 08193 Bellaterra, Spain*

† Electronic Supplementary Information (ESI) available: movies of the preliminary reconstruction and the BSS 3D components, as well as further information about the experimental and the MVA.

1 V. J. Folen, G. T. Rado and E. W. Stalder, *Phys. Rev. Lett.,* 1961, **6**, 607-608 (DOI:10.1103/PhysRevLett.6.607).
2 G. T. Rado and V. J. Folen, *Phys. Rev. Lett.,* 1961, **7**, 310-311 (DOI:10.1103/PhysRevLett.7.310).
3 R. Ramesh and N. A. Spaldin, *Nature Materials,* 2007, **6**, 21-29 (DOI:10.1038/nmat1805).
4 C. Nan, M. I. Bichurin, S. Dong, D. Viehland and G. Srinivasan, *J. Appl. Phys.,* 2008, **103**, 031101 (DOI:10.1063/1.2836410).
5 L. Yan, Y. Yang, Z. Wang, Z. Xing, J. Li and D. Viehland, *J. Mater. Sci.,* 2009, **44**, 5080-5094 (DOI:10.1007/s10853-009-3679-1).
6 N. Dix, R. Muralidharan, J. Rebled, S. Estrade, F. Peiro, M. Varela, J. Fontcuberta and F. Sanchez, *Acs Nano,* 2010, **4**, 4955-4961 (DOI:10.1021/nn101546r).
7 H. Zheng, J. Wang, S. Lofland, Z. Ma, L. Mohaddes-Ardabili, T. Zhao, L. Salamanca-Riba, S. Shinde, S. Ogale, F. Bai, D. Viehland, Y. Jia, D. Schlom, M. Wuttig, A. Roytburd and R. Ramesh, *Science,* 2004, **303**, 661-663 (DOI:10.1126/science.1094207).
8 H. Zheng, Q. Zhan, F. Zavaliche, M. Sherburne, F. Straub, M. P. Cruz, L. Chen, U. Dahmen and R. Ramesh, *Nano Lett.,* 2006, **6**, 1401-1407 (DOI:10.1021/nl060401y).
9 H. Zheng, J. Wang, L. Mohaddes-Ardabili, M. Wuttig, L. Salamanca-Riba, D. G. Schlom and R. Ramesh, *Appl. Phys. Lett.,* 2004, **85**, 2035-2037 (DOI: 10.1063/1.1786653).
10 F.Zavaliche, H. Zheng, L. Mohaddes-Ardabili, S. Y. Yang, Q. Zhan, P. Shafer, E. Reilly, R. Chopdekar, Y. Jia, P. Wright, D. G. Schlom, Y. Suzuki and R. Ramesh, *Nano Letters,* 2005, **5**, 1793-1796 (DOI: 10.1021/nl051406i).
11 F. Zavaliche, T. Zhao, H. Zheng, F. Straub, M. P. Cruz, P. -. Yang, D. Hao and R. Ramesh, *Nano Letters,* 2007, **7**, 1586-1590 (DOI: 10.1021/nl070465o).
12 I. Levin, J. Slutsker, J. Li, Z. Tan and A. L. Roytburd, *Appl. Phys. Lett.,* 2007, **91**, 062912 (DOI: 10.1063/1.2768890).

13 I. Levin, J. Li, J. Slutsker and A. L. Roytburd, *Adv Mater,* 2006, **18**, 2044-2047(DOI: 10.1002/adma.200600288).

14 J. Slutsker, Z. Tan, A. L. Roytburd and I. Levin, *J. Mater. Res.,* 2007, **22**, 2087-2095 (DOI: 10.1557/JMR.2007.0286).

15 Q. Zhan, R. Yu, S. P. Crane, H. Zheng, C. Kisielowski and R. Ramesh, *Appl. Phys. Lett.,* 2006, **89**, 172902.

16 J. Li, I. Levin, J. Slutsker, V. Provenzano, P. K. Schenck, R. Ramesh, J. Ouyang and A. L. Roytburd, *Appl. Phys. Lett.,* 2005, **87**, 072909 (DOI: 10.1063/1.2031939).

17 S. Ren, R. M. Briber and M. Wuttig, *Appl. Phys. Lett.,* 2008, **93**, 173507 (DOI: 10.1063/1.3005558).

18 J. X. Zhang, J. Y. Dai, W. Lu, H. L. W. Chan, B. Wu and D. X. Li, *J. Phys. D,* 2008, **41**, 235405 (DOI: 10.1088/0022-3727/41/23/235405).

19 R. Bachelet, F. Sanchez, J. Santiso, C. Munuera, C. Ocal and J. Fontcuberta, *Chem. Mat.,* 2009, **21**, 2494-2498 (DOI:10.1021/cm900540z).

20 G. Möbus, R. C. Doole and B. J. Inkson, *Ultramicroscopy,* 2003, **96**, 433-451 (DOI:DOI: 10.1016/S0304-3991(03)00106-2).

21 M. Weyland and P. A. Midgley, *Microscopy and Microanalysis,* 2003, **9**, 542-555 (DOI:10.1017/S1431927603030162).

22 R. D. Leapman, E. Kocsis, G. Zhang, T. L. Talbot and P. Laquerriere, *Ultramicroscopy,* 2004, **100**, 115-125 (DOI:DOI: 10.1016/j.ultramic.2004.03.002).

23 K. Jarausch, P. Thomas, D. N. Leonard, R. Twesten and C. R. Booth, *Ultramicroscopy,* 2009, **109**, 326-337 (DOI:DOI: 10.1016/j.ultramic.2008.12.012).

24 L. Yedra, A. Eljarrat, R. Arenal, E. Pellicer, M. Cabo, A. Lopez-Ortega, M. Estrader, J. Sort, M. Dolors Baró, S. Estradé and F. Peiró, *Ultramicroscopy,* 2012, **122**, 12-18 (DOI:10.1016/j.ultramic.2012.07.020).

25 C. Jeanguillaume, P. Trebbia and C. Colliex, *Ultramicroscopy,* 1978, **3**, 237-242 (DOI:10.1016/S0304-3991(78)80030-8).

26 M. H. Gass, K. K. K. Koziol, A. H. Windle and P. A. Midgley, *Nano Letters,* 2006, **6**, 376-379 (DOI:10.1021/nl052120g).

27 N. Dobigeon, S. Moussaoui, M. Coulon, J. Tourneret and A. O. Hero, *Ieee Transactions on Signal Processing,* 2009, **57**, 4355-4368 (DOI:10.1109/TSP.2009.2025797).

28 F. de la Peña, M. -. Berger, J. -. Hochepied, F. Dynys, O. Stephan and M. Walls, *Ultramicroscopy,* 2011, **111**, 169-176 (DOI:DOI: 10.1016/j.ultramic.2010.10.001).

29 R. Arenal, F. de la Peña, O. Stéphan, M. Walls, M. Tencé, A. Loiseau and C. Colliex, *Ultramicroscopy,* 2008, **109**, 32-38 (DOI:DOI: 10.1016/j.ultramic.2008.07.005).

30 P. Gilbert, *J. Theor. Biol.,* 1972, **36**, 105-117 (DOI:DOI: 10.1016/0022-5193(72)90180-4).

31 R. N. Cochran and F. H. Horne, *Anal. Chem.,* 1977, **49**, 846-853 (DOI:10.1021/ac50014a045).

32 M. Miller, K. Russell and G. Thompson, *Ultramicroscopy,* 2005, **102**, 287-298 (DOI:10.1016/J.ULTRAMIC.2004.10.011).

33 B. Goris, S. Bals, W. Van den Broek, J. Verbeeck and G. Van Tendeloo, *Ultramicroscopy,* 2011, **111**, 1262-1267 (DOI:10.1016/j.ultramic.2011.02.007).

34 P. Cueva, R. Hovden, J. A. Mundy, H. L. Xin, and D. A. Muller, *Microscopy and Microanalysis*, 2012, **18**, 4, 667-675 (DOI: 10.1017/S1431927612000244).